Calculation of Three-Dimensional Shock/Turbulent Boundary-Layer Interaction Generated by Sharp Fin

Doyle D. Knight*

Rutgers, The State University of New Jersey, New Brunswick, New Jersey

A three-dimensional oblique shock/turbulent boundary-layer interaction is computed using a hybrid explicit-implicit numerical algorithm for the compressible Navier-Stokes equations. The flow configuration consists of a sharp fin or wedge, attached normal to a flat plate. The deflection of the wedge generates an oblique shock wave that interacts with the turbulent boundary layer on the flat plate. Computed results are obtained at Mach number $M_\infty = 3$ for a wedge angle of 10 deg and Reynolds number of $Re_{\delta_\infty} = 2.8 \times 10^5$ based on the undisturbed boundary-layer thickness δ_∞ upstream of the sharp fin. These results, together with the results of a previous computation for the same configuration at $Re_{\delta_\infty} = 9.3 \times 10^5$, are compared to the recent experimental data of McClure and Dolling. The computed results are in generally good agreement with the experiment and predict with reasonable accuracy the recovery of the boundary layer to a nominal two-dimensional state downstream of the interaction. Contour plots of various flow variables are employed to investigate the flow structure for the $Re_{\delta_\infty} = 2.8 \times 10^5$ case and to compare with the model developed by Oskam, et al. based upon experimental measurements at $Re_{\delta_\infty} = 9.3 \times 10^5$.

Introduction

THE understanding of two- and three-dimensional shock wave/turbulent boundary-layer interactions (denoted as "2D" or "3D turbulent interactions") remains an important research effort in fluid dynamics. In aerodynamics, important examples of 3D turbulent interactions include transonic airfoils, supersonic inlets, nozzles, and deflected control surfaces and wing/body junctures at transonic and supersonic speeds.[1,2] In other applications in fluid dynamics (e.g., gasdynamic lasers[3]), 3D turbulent interactions are important as well. A brief sampling of recent experimental and theoretical research is given in Ref. 4.

The present research concerns the numerical simulation of a 3D oblique shock/turbulent boundary-layer interaction for the geometric configuration shown in Fig. 1. The theoretical model is the three-dimensional mean compressible Navier-Stokes equations, with turbulence incorporated using the algebraic turbulent eddy viscosity model of Baldwin and Lomax.[5] An oblique shock wave, generated by the deflection of a sharp fin mounted perpendicular to a flat plate, intersects a supersonic equilibrium turbulent boundary layer that has developed on the flat plate. The configuration, denoted the "3D sharp fin," has been investigated experimentally at a variety of freestream conditions.[6-13] In the present study, the flowfield has been computed for a nominal freestream Mach number $M_\infty = 3$, nominal wedge angle $\alpha_g = 10$ deg, and Reynolds number $Re_{\delta_\infty} = 2.8 \times 10^5$, where $Re_{\delta_\infty} = \rho_\infty U_\infty \delta_\infty / \mu_\infty$ and δ_∞ is the boundary layer thickness on the flat plate upstream of the sharp fin leading edge. In a previous study by the author,[4] the same configuration was computed at a higher Reynolds number $Re_{\delta_\infty} = 9.3 \times 10^5$. Overall, the strength of the interaction is modest, with a theoretical pressure rise of 2.02.

The first objective of the present research is to determine the capability of the theoretical model to predict the experi-

mental flowfield examined by McClure and Dolling[13,14] at two Reynolds numbers. In particular, the experimental data for the $Re_{\delta_\infty} = 2.8 \times 10^5$ case permit scrutiny of the model's ability to predict the recovery of the boundary layer on the flat plate to a nominal two-dimensional state far downstream of the shock. Specifically, boundary-layer profiles of pitot pressure and yaw angle on the flat plate were measured at distances as large as 53 δ_∞ downstream of the sharp fin leading edge. In both the previous study[4] by the present author at $Re_{\delta_\infty} = 9.3 \times 10^5$ and the study of Horstman and Hung[15] using the Escudier[16] turbulence model for the same configuration at $Re_{\delta_\infty} = 8.7 \times 10^5$, the experimental boundary layer data[9-11] were available only for $x \leq 14\delta_\infty$. The determination of capability of the theoretical model to predict the downstream recovery of the boundary layer in this case is particularly important since 1) the Baldwin-Lomax model is widely used in computational fluid dynamics and 2) the Baldwin-Lomax model, like other algebraic turbulence models, does not accurately predict the recovery of a turbulent boundary layer downstream of a strong *two-dimensional* turbulent interaction.[17]

The second objective is to examine the structure of the computed flowfield contingent upon a successful comparison with the available experimental data. In particular, it is desired to compare the computed flowfield structure at $Re_{\delta_\infty} = 2.8 \times 10^5$ with the flow model developed by Oskam, Vas, and Bogdonoff[9,10] based upon experimental measurements at $Re_{\delta_\infty} = 9.3 \times 10^5$.

Method of Solution

The details of the solution technique are given in Ref. 4 and, therefore, will only be summarized here. A coordinate transformation is employed to efficiently handle the computational domain. The governing equations are the full mean compressible Navier-Stokes equations in three dimensions using mass-averaged variables and strong conservation form. The turbulent eddy viscosity model of Baldwin and Lomax[5] is employed, with additional modifications to handle the corner region formed by the wedge and plate. The hybrid explicit-implicit numerical algorithm of Knight,[4] incorporating the explicit method of MacCormack[18] and the implicit box scheme of Keller,[19] is employed to solve the governing equations. The

*Professor, Department of Mechanical and Aerospace Engineering. Associate Fellow AIAA.
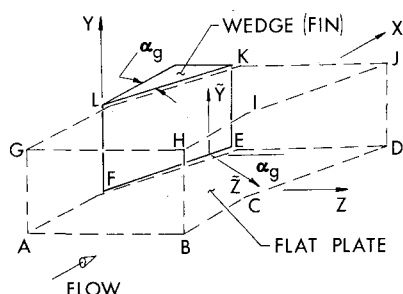
Fig. 1 Three-dimensional sharp fin configuration.

Fig. 2 Experimental data stations of Oskam.

algorithm was vectorized and executed on the Cyber 203 computer at NASA Langley. The algorithm has been previously applied to a variety of 2D and 3D shock/turbulent boundary-layer interactions.[4]

Results

Description of Flow Conditions

The flow geometry, detailed in Fig. 1, has been extensively surveyed at approximately Mach 3 for a range of values of the wedge angle α_g and upstream boundary-layer thickness δ_∞ by Oskam et al.[9-11] and McClure and Dolling.[13,14] The experimental data of Oskam et al. includes measurements of surface pressure and heat transfer on the flat plate and profiles of the pitot pressure and yaw angle [defined as $\tan^{-1}(w/u)$, where u and w are the components of the velocity in the x and z directions, respectively (Fig. 1)] for the boundary layer on the flat plate. The location of the Oskam data stations for $\alpha_g = 10$ deg are shown in Fig. 2. For the $\alpha_g = 10$ deg case, boundary-layer profiles were obtained by Oskam et al. at $Re_{\delta\infty} = 9.3 \times 10^5$ only. The experimental data of McClure and Dolling include measurements of the surface and pitot pressures and yaw angle profiles for the flat-plate boundary layer at two Reynolds numbers, namely, $Re_{\delta\infty} = 2.8 \times 10^5$ and 8.0×10^5. As shown in Fig. 3, the boundary-layer profiles were obtained in a plane parallel to the direction of the oncoming flow. This differs from the approach used by Oskam (Fig. 2), in which the profiles were obtained in planes normal to the direction of the oncoming flow. The locations of the profile measurements of McClure and Dolling were chosen to provide greater detail in the vicinity of the shock wave. The number of profiles each for yaw and pitot pressure was 21 and 22 at $Re_{\delta\infty} = 2.8 \times 10^5$ and 8.0×10^5, respectively.

In the previous study by the author,[4] computed results were obtained at Mach 3 for $\alpha_g = 10$ deg at $Re_{\delta\infty} = 9.3 \times 10^5$. These results were compared with the experimental data of Oskam et al.[9-11] In general, good agreement was obtained in comparison with the entire range of experimental data.

In the present effort, two separate computations (denoted later as grids 1 and 2) were performed at Mach 3 for $\alpha_g \cong 10$ deg at $Re_{\delta\infty} = 2.8 \times 10^5$. These two calculations are denoted as case 1. The values of the freestream conditions are indicated in Table 1 and are in agreement with the experimental test conditions of McClure and Dolling for this case, as shown in Table 2.

In the present paper, the previous computed results of the author[4] at Mach 3, $\alpha_g \cong 10$ deg and $Re_{\delta\infty} = 9.3 \times 10^5$ are compared with the experimental data of McClure and Dolling at these approximate conditions. These results are denoted as case 2 in Table 1 and the corresponding experimental test conditions of McClure and Dolling are shown in Table 2. There is a slight difference in the value of $Re_{\delta\infty}$ for case 2 between the computation and the experiment. This is attributable to the fact that the freestream conditions in the computation for case 2 were chosen to closely match the experimental conditions of Oskam et al.[9-11]
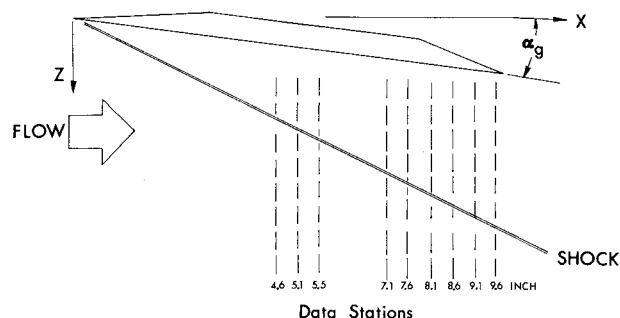
Table 1 Flow conditions for computations

Case no.	δ_∞, cm	M_∞	α_g	$Re_{\delta\infty}$	Total Pressure, kPa	Total Temperature, K
1	0.45	2.91	10.0	2.75×10^5	689.7	275.9
2	1.37	2.94	9.72	9.25×10^5	689.7	255.6

Table 2 Flow conditions for experiments of McClure and Dolling[14]

Case no.	δ_∞, cm	M_∞	α_g	$Re_{\delta\infty}$	Total pressure, kPa	Total Temperature, K
1	0.45	2.91	10.0	2.75×10^5	689.7	275.9
2	1.29	2.93	10.0	8.0×10^5	689.9	271.4

In all computations, the flat-plate surface temperature is 280.6 K. The wedge surface temperature for the computations is 280.6 and 252.8 K for cases 1 and 2, respectively. These values were chosen based on the experimental conditions and are close to adiabatic conditions.

Details of Computations

The boundary-layer profile on the upstream plane (ABHG in Fig. 1) is obtained by computing the development of a flat-plate turbulent boundary layer to the point where the computed momentum thickness θ_∞ is equal to the experimental value ($\theta_\infty = 0.030$ and 0.065 cm for cases 1 and 2, respectively). At this location, the computed and measured displacement thickness δ^*_∞ agree within 2% for both cases ($\delta^*_\infty = 0.16$ and 0.34 cm for cases 1 and 2, respectively). The computed and measured values of the skin-friction coefficient c_f agree within 2.2% for both cases ($c_f = 1.36 \times 10^{-3}$ and 1.08×10^{-3} for cases 1 and 2, respectively). The computed and measured values of the boundary-layer thickness are in close agreement (see Table 2 for experimental values) and the velocity profiles are in close agreement with the law of the wall and wake.[20]

Two separate computations were performed for case 1 ($Re_{\delta\infty} = 2.8 \times 10^5$). In each of these computations, the numerical grid incorporated 58 points in the ξ direction, 54 points in the η direction, and 34 points in the ζ direction (see Fig. 2 of Ref. 4), as indicated in Table 3. The total number of grid points in the η and ζ directions are equal to the sum of the ordinary and sublayer grid points, less the two points coinciding at the surface and edge of the sublayer. The total number of grid points for each computation (including the computational sublayer) is 106,316. The details of the grid resolution are shown in Table 4. The streamwise grid spacing Δx is uniform and equal to 1.12 δ_∞. Previous experience[4] has indicated that $\Delta x \cong \delta_\infty$ provides accurate streamwise resolution for this configuration. The grid spacing in the cross plane was a combination of a geometrically stretched and uniformly

spaced mesh in the y and z directions, with accurate resolution of the boundary layers on the wedge and flat plate and the inviscid region of the flow. In particular, the height of the first grid point adjacent to the wedge and flat plate was less than 3.1 wall units at all locations (i.e., $\Delta z_2'^+ \leq 3.1$, where $\Delta z_2'^+ = \Delta z_2' u_*/\nu_w$, $\Delta z_2'$ is the distance of the first row of points in the computational sublayer from the flat plate, u_* the wall friction velocity, and ν_w the wall kinematic viscosity). These two separate computations differed only in the height z_m' of the "computational sublayer"[4] on the flat plate. Specifically, the height z_m' was 7.62×10^{-3} cm and 1.22×10^{-2} cm for grids 1 and 2, respectively. These values correspond to 29.2 and 46.2 wall units, respectively, based upon the upstream skin friction on the plate. The solutions using grids 1 and 2 were examined to determine the sensitivity of the computed flowfield to the height of the computational sublayer and the results were found to be essentially identical. This result again confirmed the insensitivity of the computed flowfield to the height z_m' within the restriction $z_m'^+ \leq 60$ as discussed in Ref. 4. The typical number of grid points within the boundary layers is 21 for the flat plate and 16 for the wedge. The maximum grid spacing in the y direction $\Delta y_\infty/\delta_\infty$ is 0.67 and 0.75, respectively, for grids 1 and 2. The height of the computational domain in the y direction is 9 δ_∞ for both grids. The width of the computational domain in the z direction increases linearly from 10.2 δ_∞ at $x = 0$ to 41.1 δ_∞ at the furthest downstream plane. Likewise, the maximum grid spacing in the z direction $\Delta z_\infty/\delta_\infty$ varies from 0.284 to 1.2 δ_∞ at the furthest downstream plane.

The numerical grid for case 2 ($Re_{\delta_\infty} = 9.3 \times 10^5$) utilized 48 points in the ξ direction, 51 points in the η direction, and 32 points in the ζ direction (Table 3). The streamwise grid spacing Δx was uniform and equal to 0.46 δ_∞ (Table 4). The grid spacing in the cross plane was a combination of a geometrically stretched and uniformly spaced mesh in the y and z directions, with accurate resolution of the boundary layers on the wedge and flat plate and the inviscid region of the flow. In particular, the height of the first grid points adjacent to the wedge and flat plate was less than 3.2 wall units at all locations. The total number of grid points (including the computational sublayer) is 79,727. Further details are provided in Ref. 4.

The initial condition for grid 2 of case 1 was obtained by extending the upstream profile to all downstream stations. The initial condition for grid 1 of case 1 was obtained from grid 2. The former case was computed for a physical time of approximately 3.4 t_c, where t_c is the time required for a fluid parcel to travel from the upstream to the downstream planes in the inviscid region. By this time, the flowfield had converged to steady state.[4] The latter case was computed for a physical time of 2.3 t_c, at which point the flowfield was converged to steady state. The computer time on the Cyber 203 for grids 1 and 2 was 4.4 and 5.0 h, respectively. The initial conditions and computer requirements for case 2 are discussed in Ref. 4.

Comparison of Theoretical and Experimental Results

A representative selection of computed and experimental pitot pressure profiles on the flat plate for cases 1 and 2 are shown in Figs. 4-7. The vertical axis is the distance normal to the flat plate, normalized by δ_∞ (Table 1). The horizontal axis is the pitot pressure p_p, normalized by the upstream freestream pitot pressure $p_{p\infty}$. The profiles are taken at a constant spanwise distance $z = 14.2$ and 9.4 δ_∞, respectively, for cases 1 and 2 (Fig. 3). The streamwise location is given in terms of
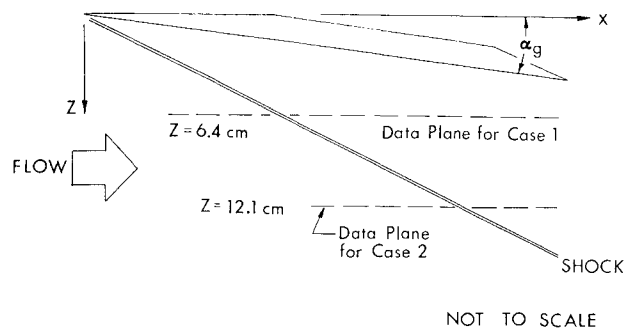

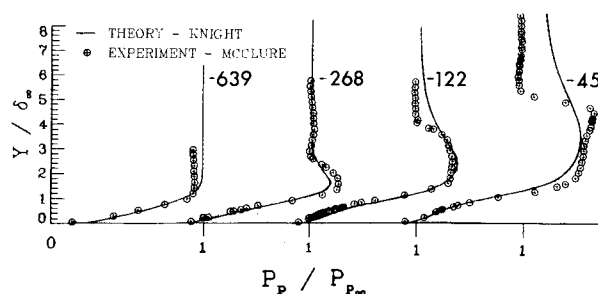Fig. 3   Experimental data stations of McClure and Dolling.

Fig. 4   Pitot pressure for case 1 at $x_s' = -639$, -268, -122, and -45.

Table 3   Details of mesh distribution[a]

Case no.	Grid no.	$Re_{\delta\infty}$	N_ξ	N_η	N_ζ	NSL[b]
1	1	2.8×10^5	58	48	28	8
1	2	2.8×10^5	58	48	28	8
2	1	9.3×10^5	48	46	27	7

[a]N_ξ, N_η, and N_ζ are the number of ordinary points in the ξ, η, and ζ directions (see Figs. 1 and 2 in Ref. 4).

[b]NSL is the number of mesh points in the z' direction in the computational sublayer (see Ref. 4).

Table 4   Details of mesh resolution

Case no.	Grid no.	Wedge[a,b]		Flat plate[c,d]				
		Max $\Delta z_2'^+$	NBL	Max $\Delta z_2'^+$	NBL	$\Delta x/\delta_\infty$	$\Delta y_\infty/\delta_\infty$	$\Delta z_\infty/\delta_\infty$
1	1	2.94	16	3.12	21	1.12	0.67	0.28-1.2
1	2	2.95	16	3.08	21	1.12	0.75	0.28-1.2
2	1	3.19	17	2.65	20	0.46	0.58	0.49

[a]Max $\Delta z_2'^+$ = maximum value of $\Delta z_2'^+$, where $\Delta z_2'^+ = \Delta z_2' u_*/\nu_w$ and $\Delta z_2'$ is the distance of the first row of sublayer points from the boundary.

[b]NBL = total number of points in the boundary layer. For the wedge, NBL is evaluated at point K in Fig. 1. For the flat plate, NBL is the number of points in the boundary layer upstream of the interaction.

[c]Δx = mesh spacing in the x direction.

[d]Δy_∞, Δz_∞ = ordinary mesh spacing in the y and z directions in the region of uniform grid.
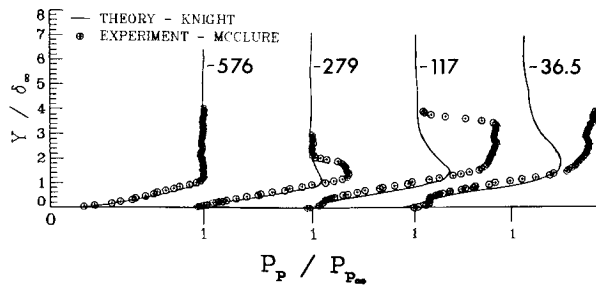
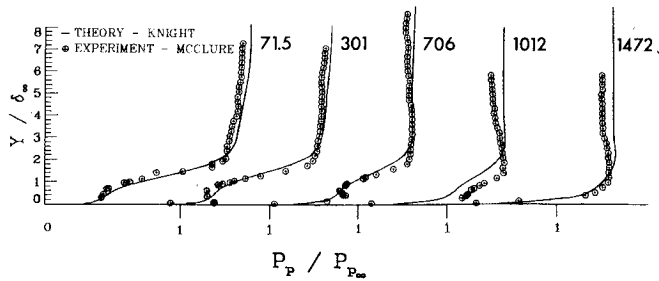Fig. 5   Pitot pressure for case 2 at $x_s' = -576, -279, -117,$ and -36.5.

Fig. 6   Pitot pressure for case 1 at $x_s' = 71.5, 301, 706, 1012,$ and 1472.
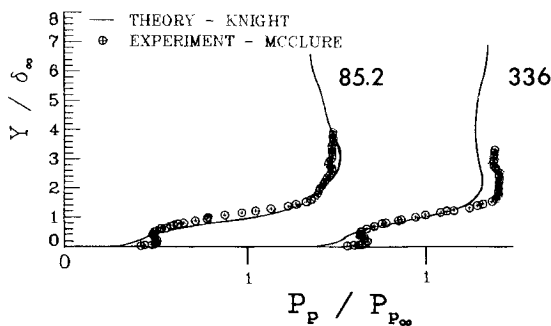

Fig. 7   Pitot pressure for case 2 at $x_s' = 85.2$ and 336.

Fig. 8   Yaw angle for case 1 at $x_s' = -639, -268, -122,$ and -45.

stream of the interaction.[9,25] The comparison between the computed and experimental profiles for case 1 is very good, with the peak value of p_p predicted within 5% for all stations. The comparison for case 2 shows greater discrepancy, with the computation failing to exhibit the full magnitude of the overshoot. This discrepancy is not attributable to grid resolution; indeed, as indicated in Table 4, the grid resolution for case 2 surpassed that of case 1. Furthermore, computations of the same cases by Horstman[26] using the $k - \epsilon$ turbulence model[27] display close agreement with the present calculations. The understanding of this discrepancy is the subject of present research.

In Figs. 6 and 7, pitot profiles are shown at several stations downstream of the theoretical shock. The profiles for case 1 are displayed at $x_s' = 71.5, 301, 706, 1012,$ and 1472. The profiles for case 2 are shown at $x_s' = 85.2$ and 336. There is generally good agreement between the theory and experiment, although the computed profiles near the wall slightly underpredict the observed p_p behavior for stations near the shock. The continued development of the p_p profiles for case 1 to $x_s' = 1472$ is seen to be in good agreement with experiment. Comparison with all other experimental pitot pressure profiles (not shown) indicates similar agreement and confirms the above conclusions.

A representative selection of computed and measured yaw angle profiles upstream of the shock wave are shown in Figs. 8-11, where the yaw angle is $\tan^{-1}(w/u)$ (see Fig. 1). Profiles upstream of the theoretical inviscid shock are displayed in Figs. 8 and 9, using the same values of x_s' as in Figs. 4 and 5. Upstream of the interaction, the yaw angle is zero. The yaw angle in the vicinity of the surface rises rapidly as the flow approaches the shock, due to the spanwise pressure gradient imposed on the flow. Within the boundary layer, the calculated and experimental profiles are in good agreement, with the theory slightly underpredicting the observations within the lower 20% of the boundary layer. Outside the boundary layer, however, a region of overshoot in the yaw angle appears. This behavior is not seen in the computation. A similar computation by Horstman[26] using the $k - \epsilon$ turbulence model is in good agreement with the present calculations and does not display the overshoot in yaw angle.

In Figs. 10 and 11, yaw angle profiles are displayed at several stations downstream of the theoretical inviscid shock. The stations x_s' are the same as in Figs. 6 and 7. General good agreement is observed between the computation and experiment, although the computed profile for case 2 modestly underpredicts the yaw angle near the wall. The asymptotic value of the yaw angle as y approaches zero is predicted reasonably well in both cases. In addition, the computed profiles accurately predict the "undershoot" in the yaw angle profile outside the boundary layer (i.e., values of the yaw angle less than the wedge angle $\alpha_g \cong 10$ deg). The continued development of the yaw angle profile for case 1 to $x_s' = 1472$ displays close agreement between theory and experiment. In particular, the decrease of the observed surface yaw angle from a maximum of approximately 40 deg in the immediate vicinity of the shock to 12 deg at $x_s' = 1472$ is accurately described by the computations. The computed value of the

x_s', where $x_s' = (x - x_{shk}) Re_{\delta_0}^{\frac{1}{3}}/\delta_0$, x_{shk} is the location of the theoretical inviscid shock wave at the specified spanwise location z, and δ_0 is the experimental flat-plate boundary-layer thickness measured at (x_{shk}, z) in the absence of the wedge. The shock location $x_{shk} = 12.0$ and 22.8 cm for cases 1 and 2, respectively. The local undisturbed boundary-layer thickness δ_0 is 0.59 and 1.55 cm, respectively. The choice of x_s' as the streamwise distance parameter is motivated by the observations of Settles et al.[21,24] and Dolling et al.,[22,23] implying that, for the fixed M_∞ and α_g of the present investigations, the surface features (e.g., limiting streamlines, surface pressure) are effectively scaled in this manner. The profiles from cases 1 and 2 are therefore selected to correspond wherever possible to approximately the same values of x_s'. McClure and Dolling[13,14] examined the extension of the scaling law to the flowfield (specifically, pitot pressure and yaw angle) and obtained promising, although not conclusive, results.

In Figs. 4 and 5, pitot pressure profiles are displayed at several locations upstream of the theoretical inviscid shock wave. The profiles for case 1 are at $x_s' = -639, -268, -122,$ and -45; those for case 2 are at $x_s' = -576, -279, -117,$ and -36.5. Beginning from the undisturbed two-dimensional boundary layer, the p_p profiles for both cases exhibit a region of overshoot ("bulge") located outside the boundary layer and upstream of the theoretical inviscid shock. This overshoot is associated with the compression region that develops up-
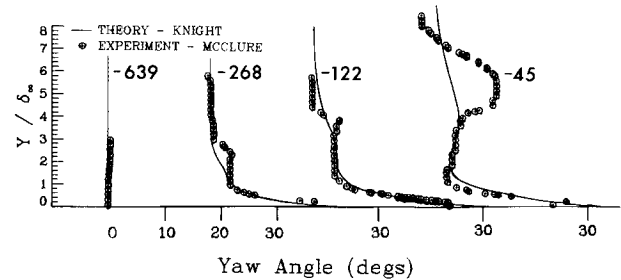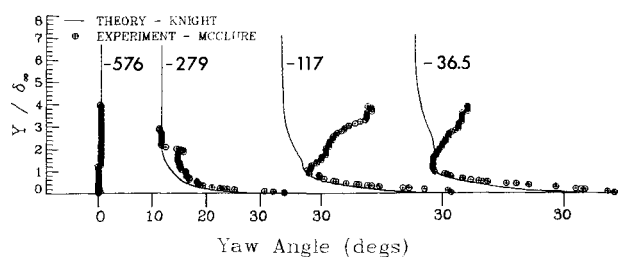
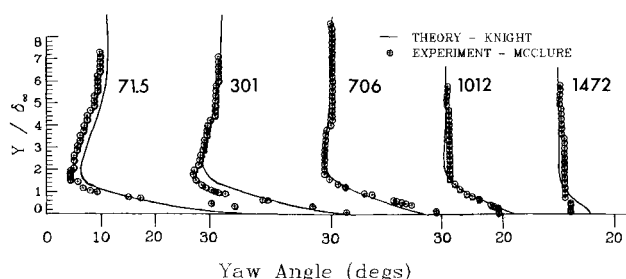Fig. 9   Yaw angle for case 2 at $x'_s = -576, -279, -117,$ and -36.5.

Fig. 10   Yaw angle for case 1 at $x'_s = 71.5, 301, 706, 1012,$ and 1472.

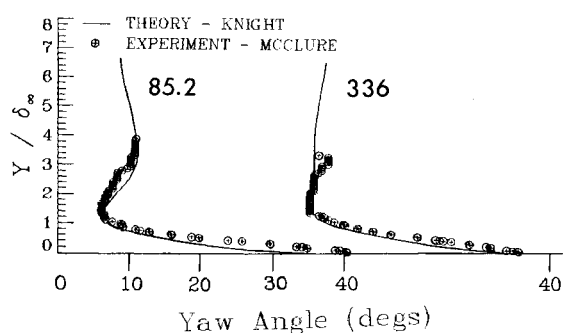Fig. 11   Yaw angle for case 2 at $x'_s = 85.2$ and 336.

Fig. 12a   Pitot pressure at $x = 57.6\delta_\infty$ ($p_p/p_{p\infty} = 0.5, 0.7, 0.9, 1.1, 1.2, 1.3, 1.4,$ and 1.5).

Fig. 12b   Yaw angle at $x = 57.6\delta_\infty$ (yaw $= 4, 6, 8, 15, 20, 25,$ and 30 deg).

Fig. 12c   Pitch angle in x-y plane at $x = 57.6\delta_\infty$ (pitch $= -1, 1, 2,$ and 3 deg).

Fig. 12d   Static pressure at $x = 57.6\delta_\infty$ ($p/p_\infty = 1.1, 1.2, \ldots, 1.9$).

surface yaw angle at $x'_s = 1472$ is 16 deg. The experimental uncertainty[13] is ± 1 deg. Comparison with all other experimental yaw angle profiles (not shown) indicates similar agreement and confirms the above conclusions.

Contour Plots at $Re_{\delta_\infty} = 2.8 \times 10^5$

Contour plots of the computed pitot pressure, yaw angle, pitch angle, and static pressure for case 1 are displayed in Fig. 12 at $x = 57.6 \; \delta_\infty$. This x station intersects the shock downstream of the "inception region"[24] and is therefore within the domain where the interaction "footprint" is conically symmetric.[24] The left boundary of each plot represents the wedge surface and the lower boundary corresponds to the flat plate, with δ denoting the local boundary-layer thickness on the flat plate in the two-dimensional region of the flow. The location of the theoretical inviscid shock at each station is indicated by the S arrow. The C arrow indicates the approximate location of the line of coalescence of the surface shear stress (i.e., limiting streamlines or "three dimensional separation line"[8]). The computed limiting streamlines for cases 1 and 2 are shown in Refs. 28 and 4, respectively.

The pitot pressure contours indicate the size of the boundary layers on the flat plate and wedge surface. The shock wave is evident in the clustering of vertical pitot contours and is situated slightly to the right of the theoretical inviscid shock position due to the displacement thickness effect of the wedge boundary layer. The shock-capturing nature of the numerical algorithm effectively "diffuses" the shock wave over typically
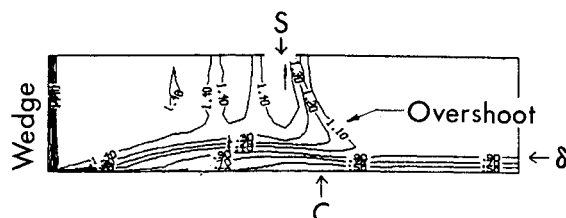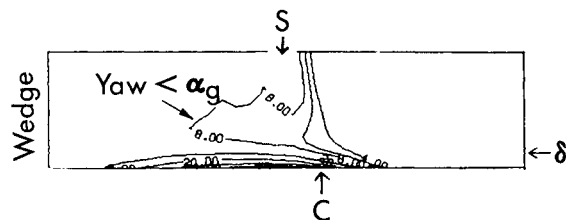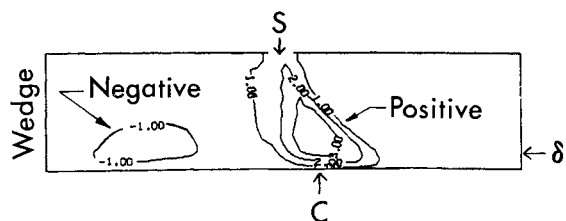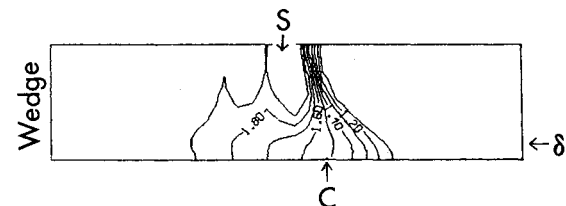
two to three grid points. The overshoot in the pitot contours, extending to the right at the intersection of the shock wave and boundary layer on the flat plate, represents the upstream propagation of the 3D turbulent interaction and was observed in Fig. 4. The particular contour $p_p/p_{p\infty} = 1.4$ displays a repeated U-shaped pattern in the region between the shock and the wedge surface and above the flat-plate boundary layer. This pattern is associated with the small variations in $p_p/p_{p\infty}$ around 1.4 in this inviscid region ($p_p/p_{p\infty}$ varies between approximately 1.35 and 1.5 in this region) and does not represent a significant structure of the flow. The decrease in boundary-layer thickness on the flat plate in the vicinity of the wedge is also evident. This effect is attributed to the large cross flow induced by the shock/boundary-layer interaction.[9,10]

The general structure agrees of the computed yaw angle for case 1 shown in Fig. 12b is in agreement with the description of Oskam et al.[9,10] based upon measurements at $Re_{\delta_\infty} = 9.3 \times 10^5$. A region of large yaw angle develops within the boundary layer on the flat plate, extending upstream of the shock location. A region of yaw angle below the wedge angle $\alpha_g = 10$ deg appears outside the boundary layer and downstream of the shock. The fluid in this region is moving toward the wedge.

The contour plot of the computed pitch angle in the x-y plane for case 1 at $x/\delta_\infty = 57.6$ is shown in Fig. 12c. The pitch angle is defined as $\tan^{-1}(v/u)$ where u and v are the Cartesian velocity components in the x and y directions,

respectively. In the vicinity of the corner formed by the flat plate and the wedge, a region of negative pitch angle is observed at all streamwise locations, in agreement with the flow model of Oskam et al. Close to the leading edge,[28] the minimum value of the pitch angle is approximately -10 deg. These regions of large negative pitch exhibit yaw angles close to $\alpha_g = 10$ deg, indicating the fluid is moving downward toward the flat plate and roughly parallel to the wedge. This downward motion acts to replenish the fluid that has been swept in the spanwise direction.[9,10] The magnitude of the negative pitch decreases with distance x and, at the station shown the minimum value of the pitch angle, is approximately -1 deg. A significant region of two-dimensional flow has developed between the fin and the shock, with yaw angles less than 16 deg and pitch angles less than 1 deg. The pitch angle contour plot also displays a region of modest positive pitch angle located to the right of the shock wave and centered approximately on the line of coalescence, with a maximum value of approximately 4 deg. This maximum value decreases with x and, at the furthest downstream station, is approximately 3 deg. It is noted that the area of largest pitch angle occurs outside the boundary layer and is associated with the overshoot in pitot pressure. Although a region of positive pitch of comparable magnitude was observed by Oskam et al. in the vicinity of the shock/boundary-layer interaction,[9,10] no information was provided concerning the pitch behavior to the right of the shock wave (i.e., equivalent to upstream of the shock).

In Fig. 12d, the computed normalized static pressure p/p_∞ is displayed. The general behavior is similar to the measurements of Oskam et al. at $Re_{\delta\infty} = 9.3 \times 10^5$, displaying the development of a constant-pressure region adjacent to the wedge surface.

Conclusions

The flowfield of a three-dimensional oblique shock/turbulent boundary-layer interaction, formed by a wedge attached normal to a flat plate, has been computed at Mach 3 for a wedge angle $\alpha_g \cong 10$ deg and Reynolds number $Re_{\delta\infty} = 2.8 \times 10^5$. The full mean compressible Navier-Stokes equations are utilized, with the turbulence incorporated through the algebraic turbulent eddy viscosity model of Baldwin and Lomax. The computed results are compared to the experimental data of McClure and Dolling for pitot pressure and yaw angle profiles and found to be generally in good agreement. The calculated pitot pressure profiles accurately display the observed "overshoot" outside the boundary layer at stations slightly upstream of the shock. The computed yaw angle profiles, however, do not manifest the observed overshoot in yaw outside the boundary layer at the same locations. The computed pitot and yaw profiles are in good agreement with the experimental data in the boundary layer at all stations and predict the recovery of the boundary layer to a nominal two-dimensional state downstream of the three-dimensional interaction with reasonable accuracy.

The results of a previous computation by the author for the same configuration at $Re_{\delta\infty} = 9.3 \times 10^5$ are compared with experimental data of McClure and Dolling. The computed pitot pressure profiles display good agreement with the experimental data within the boundary layer. The calculated overshoot in pitot pressure, however, is in only qualitative agreement with experiment. The computed yaw angle profiles are likewise in good agreement with experiment within the boundary layer, although underpredicting the yaw in the lower 20% of the boundary layer. However, the asymptotic surface yaw angle is predicted with reasonable accuracy. The computed yaw profiles do not display the observed overshoot outside the boundary layer at stations upstream of the shock.

The computed flowfield at $Re_{\delta\infty} = 2.8 \times 10^5$ is analyzed and compared to the flowfield model developed by Oskam et al. based upon their measurements at $Re_{\delta\infty} = 9.3 \times 10^5$. In

general, the computed flow exhibits the same basic features as the Oskam model. The calculated flowfield also provides additional detail concerning the pitch angle behavior in the vicinity of the intersection of the shock wave and the flat plate and the region of observed "overshoot" in the pitot pressure.

Acknowledgments

References

[1] Green, J., "Interactions Between Shock Waves and Turbulent Boundary Layers," *Progress in Aeronautical Sciences*, Vol. 11, 1970, pp. 235-340.

[2] Hankey, W. and Holden, M., "Two-Dimensional Shock Wave-Boundary Layer Interactions in High Speed Flows," AGARDograph No. 203, June 1975.

[3] Christiansen, W., Russell, D., and Hertzberg, A., "Flow Lasers," *Annual Review of Fluid Mechanics*, Vol. 7, 1975, pp. 115-140.

[4] Knight, D., "A Hybrid Explicit-Implicit Numerical Algorithm for the Three-Dimensional Compressible Navier-Stokes Equations," *AIAA Journal*, Vol. 22, 1984, pp. 1056-1063.

[5] Baldwin, B. and Lomax, H., "Thin Layer Approximation and Algebraic Model for Separated Flows," AIAA Paper 78-257, 1978.

[6] McCabe, A., "The Three-Dimensional Interaction of a Shock Wave with a Turbulent Boundary Layer," *The Aeronautical Quarterly*, Vol. 17, 1966, pp. 231-252.

[7] Law, C., "Three-Dimensional Shock Wave-Turbulent Boundary Layer Interactions at Mach 6," ARL-TR-75-0191, WP AFB, OH, June 1975.

[8] Peake, D., "Three Dimensional Swept Shock/Turbulent Boundary Layer Separations with Control by Air Injection," National Research Council—Canada, Aero. Rept. LR-592, July 1976.

[9] Oskam, B., Vas, I., and Bogdonoff, S., "Mach 3 Oblique Shock Wave/Turbulent Boundary Layer Interactions in Three Dimensions," AIAA Paper 76-336, 1976.

[10] Oskam, B., Vas, I., and Bogdonoff, S., "An Experimental Study of Three-Dimensional Flow Fields in an Axial Corner at Mach 3," AIAA Paper 77-689, 1977.

[11] Oskam, B., Vas, I., and Bogdonoff, S., "Oblique Shock Wave/Turbulent Boundary Layer Interactions at Mach 3," AFFDL-TR-76-48, Pt. I, 1976, and Pt. II, 1978.

[12] Kubota, H. and Stollery, J., "An Experimental Study of the Interaction Between a Glancing Shock Wave and a Turbulent Boundary Layer," *Journal of Fluid Mechanics*, Vol. 116, March 1982, pp. 431-458.

[13] McClure, W., "An Experimental Study into the Scaling of an Unswept Sharp-Fin-Generated Shock/Turbulent Boundary Layer Interaction," M.S.E. Thesis, Dept. of Aerospace and Mechanical Engineering, Princeton University, Princeton, NJ, 1983.

[14] McClure, W. and Dolling, D., "Flowfield Scaling in Sharp Fin-Induced Shock Wave Turbulent Boundary Layer Interaction," AIAA Paper 83-1754, 1983.

[15] Horstman, C. and Hung C., "Computation of Three-Dimensional Separated Flows at Supersonic Speeds," AIAA Paper 79-0002, 1979.

[16] Escudier, M., "The Distribution of the Mixing Length in Turbulent Flows Near Walls," Mechanical Engineering Dept., Imperial College, London, Rept. TWF/TN/1, 1965.

[17] Visbal, M. and Knight, D., "The Baldwin-Lomax Turbulence Model for Two-Dimensional Shock Wave Turbulent Boundary Layer Interactions," *AIAA Journal*, Vol. 22, 1984, pp. 921-928.

[18] MacCormack, R., "Numerical Solution of the Interaction of a Shock Wave with a Laminar Boundary Layer," *Lecture Notes in Physics*, Vol. 8, 1971, pp. 151-163.

[19] Keller, H., "Accurate Difference Methods for Nonlinear Two-Point Boundary Value Problems," *SIAM Journal of Numerical Analysis*, Vol. 11, 1974, pp. 305-320.

[20] Sun, C.-C. and Childs, M., "Wall-Wake Velocity Profile for Compressible Nonadiabatic Flows," *AIAA Journal*, Vol. 14, 1976, pp. 820-822.

[21] Settles, G. and Bogdonoff, S., "Scaling of Two- and Three-Dimensional Shock/Turbulent Boundary-Layer Interactions at Compression Corners," *AIAA Journal*, Vol. 20, 1982, pp. 782-789.

[22] Dolling, D. and Bogdonoff, S., "Upstream Influence Scaling of Sharp Fin-Induced Shock Wave Turbulent Boundary Layer Interactions," AIAA Paper 81-0336, Jan. 1981.

[23] Dolling, D. and Bogdonoff, S., "Upstream Influence in Sharp Fin-Induced Shock Wave Turbulent Boundary Layer Interaction," *AIAA Journal*, Vol. 21, 1983, pp. 143-145.

[24] Lu, F. and Settles, G., "Conical Similarity of Shock/Boundary Layer Interactions Generated by Swept Fins," AIAA Paper 83-1756, 1983.

[25] Oskam, B., "Three-Dimensional Flow Fields Generated by the Interaction of a Swept Shock Wave with a Turbulent Boundary

Layer," Princeton Gas Dynamics, Rept. 1313, 1976.

[26] Knight, D., "Modelling of Three-Dimensional Shock Wave Turbulent Boundary Layer Interactions," in *Lecture Notes in Physics*, Vol. 230, pp. 177-201, Springer-Verlag, New York, 1985.

[27] Jones, W. and Launder, B., "The Prediction of Laminarization with a Two-Equation Model of Turbulence," *International Journal of Heat and Mass Transfer*, Vol. 15, 1972, pp. 301-304.

[28] Knight, D., "Numerical Simulation of 3-D Shock Turbulent Boundary Layer Interaction Generated by a Sharp Fin," AIAA Paper 84-1559, 1984.